Spatiotemporal ghost imaging and interference

Adeel Abbas,[1] Chenni Xu,[1] and Li-Gang Wang[1,2,*]
[1]*Department of Physics, Zhejiang University, Hangzhou 310027, China*
[2]*Zhejiang Province Key Laboratory of Quantum Technology and Device, Zhejiang University, Hangzhou 310027, China*

(Received 12 November 2019; revised manuscript received 5 March 2020; accepted 9 March 2020; published 7 April 2020)

Ghost imaging retrieves the image of an object by using second-order correlation, and this technique studied so far has been considered in either a spatial or temporal domain, which is hard to apply to the scenario of imaging spatiotemporal dynamic objects (STDOs). Here we propose to demonstrate spatiotemporal ghost imaging and interference (STGII) for STDOs by extending the correlation theory of optical coherence into the spatiotemporal domain. We have derived the generalized analytical formula for such STGII with partially coherent pulsed beams. Through a simple example of spatiotemporal slits at different location and time, the interesting phenomena of STGII are achieved under suitable conditions and it is observed that the image quality and interference visibility are affected by both the spatial and temporal parameters of partially coherent pulsed beams.

DOI: 10.1103/PhysRevA.101.043805

I. INTRODUCTION

Ghost imaging is an indirect imaging technique realized about two decades ago [1,2]. It was initially used for producing the spatial image of an object through correlation measurement [1–3]. The advantage of ghost imaging over conventional direct imaging consists in the permission for imaging the objects located in optically harsh and noisy environments, where conventional techniques are likely to fail, and therefore this unconventional phenomenon has potential applications in quantum metrology, lithography, and holography [4–9] . In recent years this phenomenon has emerged several important imaging technologies and has been extended to hard x rays [10,11], cold atoms [12], ultracold atoms [13], electrons [14], and neutrons [15].

From the first experiments performed with entangled two-photon pairs [1,2], ghost imaging and interference were considered as a unique phenomenon in quantum light fields [9,16]. Later, similar effects were achieved by using classical incoherent light fields but with less visibility [17,18]. In the past two decades, a good deal of attention has been given to these phenomena both theoretically and experimentally with classical incoherent or thermal light in a spatial domain [19–38]. By taking into account space-time duality in optics, the extension of spatial ghost imaging and interference to the time domain has consequently been investigated with entangled photons [39,40] and classical correlated light sources [41–47]. Temporal ghost imaging [42,43] and interference [41] with classical light pulses have also been introduced theoretically as a temporal counterpart of conventional ghost imaging. Very recently, temporal ghost imaging was experimentally realized by using a multimode laser source which achieved temporal resolution at a picosecond level [44]. The temporal ghost imaging is attractive for dynamic imaging of a temporal object with high time resolution by using the temporal correlation of ultrafast waveforms, and it is thought to be useful in phase-space tomography [42], biomedical optics [43], and improved telecommunications [44].

Conventional ghost imaging techniques can only get the image of stationary objects in spatial or temporal domains, for example, in spatial ghost imaging, an object is stationary in the temporal domain and, in temporal ghost imaging, an object has no spatial information. Spatiotemporal dynamic objects (STDOs) like biological organs, etc., may have spatial and temporal information simultaneously; for imaging such objects there is a need for an advancement in the conventional ghost imaging techniques in the spatial or temporal domain to the spatiotemporal domain. Very recently, there is a proposal to sense the angular rotation of structured objects by using the ghost image of two-photon entanglement [48]. In this work, we present a theoretical proposal for the spatiotemporal ghost imaging and interference (STGII) technique by using partially coherent spatiotemporal pulsed light sources. This technique enables us to find a dynamic ghost image and interference of STDOs which was not possible with conventional ghost imaging techniques. In order to realize such techniques, we use a partially coherent Gaussian Schell-model pulsed beam [49], which is a partially coherent spatiotemporal light field, as the source to study ghost imaging technology in a spatiotemporal domain. Based on optical coherence theory, a generalized analytical solution of STGII for a STDO is derived and the corresponding visibility is illustrated through a numerical example. Meanwhile, the effects of source properties on the visibility as well as on the pattern of fringes of such STGII are also demonstrated.

The paper is organized as follows. In Sec. II, by the use of a Gaussian Schell-model pulsed beam as source we will propose the STGII for STDOs. In Sec. III, we will discuss results with a numerical example of a two-dimensional case; the visibility and the quality of STGII will be investigated. Finally, we shall conclude our paper in the last section.

*sxwlg@yahoo.com

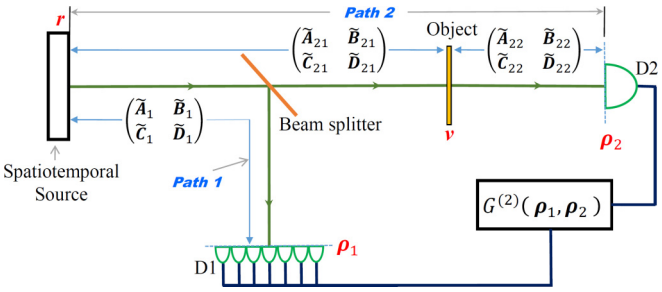

FIG. 1. Schematic of STGII. Paths 1 and 2 are test and reference arms, respectively. Every matrix in optical paths denotes all optical elements in each part. The coordinates of $\boldsymbol{r}$, $\boldsymbol{v}$, $\boldsymbol{\rho}_i$ $(i = 1, 2)$ show the spatiotemporal points at source, object, and detector planes, respectively. D1 detector should have space and time resolution and D2 is a bucket detector.

II. MODEL AND FORMULISM

As shown in Fig. 1, the system is very similar to previous ones [1,2,36,41,43], which generate spatial or temporal ghost image and interference, but here it is assumed that the detector D1 should have the ability to collect the spatial and temporal information, simultaneously, and the object may have both the space and time information. In order to perform such STGII, a partially coherent spatiotemporal pulsed beam is used as the source, which is split into two pulsed beams. One follows optical path 1 and its random fluctuation in space and time is measured by D1, which may consist of an array of the photodiodes with the fast response time much smaller than the single pulse duration, and the spatial information can be provided by the position of each photodiode in D1, while another one passes through the dynamic object and is detected by D2, which is a slow-response photodiode and cannot resolve the temporal structure of the pulse fluctuation and also does not need to provide the spatial information. From both detectors the spatiotemporal intensities are correlated via the second-order correlator.

According to the theory of optical coherence, the second-order intensity-intensity correlation function between two detectors can be expressed as [36,49]

$$G^{(2)}(\boldsymbol{\rho}_1, \boldsymbol{\rho}_2) = \langle I_1(\boldsymbol{\rho}_1)\rangle\langle I_2(\boldsymbol{\rho}_2)\rangle + |\Gamma(\boldsymbol{\rho}_1, \boldsymbol{\rho}_2)|^2, \tag{1}$$

where $I_i(\boldsymbol{\rho}_i)$ is the instantaneous intensity of the pulsed beam arriving at the ith detector and $\langle\cdot\rangle$ denotes the ensemble average. Here $\boldsymbol{\rho}_i = (x_i, y_i, \tau_i)^{\mathrm{T}}$ with $i = 1, 2$ represent two arbitrary spatiotemporal points at the measurement planes of D1 and D2, respectively, and the superscript "T" denotes the transposed operator. Here variable transformation is used as $\tau = v_{\mathrm{g}}(t - z/v_{\mathrm{g}})$, where t is the pulse arrival time, z is the distance from the source plane, $v_{\mathrm{g}} = c/n_{\mathrm{g}}$ is the group velocity of pulsed beam, c is the speed of light in vacuum, and n_{g} is the group index of medium. The assumption that the time coordinate is measured in the reference frame moving with the group velocity of the pulses has been made. Note that the first term on the right-hand side serves as the background, while the first-order spatiotemporal correlation $\Gamma(\boldsymbol{\rho}_1, \boldsymbol{\rho}_2)$ is the kernel that makes the STGII possible. By using the spatiotemporal point spread function of a linear optical system, the ensemble averaged intensities at D1 and D2 are given by

$$\langle I_i(\boldsymbol{\rho}_i)\rangle = \iiint\iiint \Gamma_0(\boldsymbol{r}_{10}, \boldsymbol{r}_{20}) \times h_i(\boldsymbol{r}_{10}, \boldsymbol{\rho}_i)h_i^*(\boldsymbol{r}_{20}, \boldsymbol{\rho}_i)d^3r_{10}d^3r_{20}, \tag{2}$$

where $\Gamma_0(\boldsymbol{r}_{10}, \boldsymbol{r}_{20})$ is the initial first-order correlation function of pulsed light fields at the source plane, the symbol "*" denotes complex conjugate, $h_i(\boldsymbol{r}, \boldsymbol{\rho}_i)$ describe the spatiotemporal point spread functions of linear optical systems, on the path 1 or path 2, which can include any linear second-order dispersion optical systems [50], and $\boldsymbol{r}_{i0} = (x_{i0}, y_{i0}, \tau_{i0})^{\mathrm{T}}$ represent the spatiotemporal points on the source plane. Meanwhile, the spatiotemporal first-order correlation between two detectors is given by

$$\Gamma(\boldsymbol{\rho}_1, \boldsymbol{\rho}_2) = \iiint\iiint \Gamma_0(\boldsymbol{r}_{10}, \boldsymbol{r}_{20}) \times h_1(\boldsymbol{r}_{10}, \boldsymbol{\rho}_1)h_2^*(\boldsymbol{r}_{20}, \boldsymbol{\rho}_2)d^3r_{10}d^3r_{20}. \tag{3}$$

We emphasize again that the above integral includes both spatial and temporal integrals on the source plane, which gives the information about spatial and temporal correlation of both detectors, respectively. More importantly, it describes the propagation properties of the first-order spatiotemporal coupling correlation when the light source has the spatiotemporal coupling characteristics. The functions $h_i(\boldsymbol{r}, \boldsymbol{\rho}_i)$ for the two paths in Fig. 1 are, respectively, given by

$$h_1(\boldsymbol{r}, \boldsymbol{\rho}_1) = \left(\frac{ik}{2\pi}\right)^{\frac{m}{2}} [\det(\widetilde{\mathbf{B}}_1)]^{-\frac{1}{2}} \exp\left[-\frac{ik}{2}\left(\boldsymbol{r}^{\mathrm{T}}\widetilde{\mathbf{B}}_1^{-1}\widetilde{\mathbf{A}}_1\boldsymbol{r} - 2\boldsymbol{r}^{\mathrm{T}}\widetilde{\mathbf{B}}_1^{-1}\boldsymbol{\rho}_1 + \boldsymbol{\rho}_1^{\mathrm{T}}\widetilde{\mathbf{D}}_1\widetilde{\mathbf{B}}_1^{-1}\boldsymbol{\rho}_1\right)\right] \tag{4}$$

for the path 1 and

$$h_2(\boldsymbol{r}, \boldsymbol{\rho}_2) = \iiint h_{21}(\boldsymbol{r}, \boldsymbol{v})h_{22}(\boldsymbol{v}, \boldsymbol{\rho}_2)d^3v \tag{5}$$

for the path 2, where $h_{21}(\boldsymbol{r}, \boldsymbol{v})$ is the point spread function from the source plane to the dynamic object, which is expressed as

$$h_{21}(\boldsymbol{r}, \boldsymbol{v}) = \left(\frac{ik}{2\pi}\right)^{\frac{m}{2}} [\det(\widetilde{\mathbf{B}}_{21})]^{-\frac{1}{2}} \exp\left[-\frac{ik}{2}\left(\boldsymbol{r}^{\mathrm{T}}\widetilde{\mathbf{B}}_{21}^{-1}\widetilde{\mathbf{A}}_{21}\boldsymbol{r} - 2\boldsymbol{r}^{\mathrm{T}}\widetilde{\mathbf{B}}_{21}^{-1}\boldsymbol{v} + \boldsymbol{v}^{\mathrm{T}}\widetilde{\mathbf{D}}_{21}\widetilde{\mathbf{B}}_{21}^{-1}\boldsymbol{v}\right)\right], \tag{6}$$

and $h_{22}(\boldsymbol{v}, \boldsymbol{\rho}_2)$ is the point spread function from the dynamic object plane to the detector D2 which can be written as

$$h_{22}(\boldsymbol{v}, \boldsymbol{\rho}_2) = \left(\frac{ik}{2\pi}\right)^{\frac{m}{2}} [\det(\widetilde{\mathbf{B}}_{22})]^{-\frac{1}{2}} H(\boldsymbol{v}) \times \exp\left[-\frac{ik}{2}\left(\boldsymbol{v}^{\mathrm{T}}\widetilde{\mathbf{B}}_{22}^{-1}\widetilde{\mathbf{A}}_3\boldsymbol{v} - 2\boldsymbol{v}^{\mathrm{T}}\widetilde{\mathbf{B}}_{22}^{-1}\boldsymbol{\rho}_2 + \boldsymbol{\rho}_2^{\mathrm{T}}\widetilde{\mathbf{D}}_{22}\widetilde{\mathbf{B}}_{22}^{-1}\boldsymbol{\rho}_2\right)\right]. \tag{7}$$

In the above equations, $k = n(\omega)\omega/c$ is the wave number of light in the system at the central frequency ω of the incident pulse, $n(\omega)$ is frequency-dependent refractive index of dispersive medium, m is the number of dimensions, and $\widetilde{\mathbf{A}}_j$, $\widetilde{\mathbf{B}}_j$, $\widetilde{\mathbf{C}}_j$,

and $\widetilde{\mathbf{D}}_j$ with $j = 1, 21, 22$ are $m \times m$ spatiotemporal transfer matrices of relevant optical systems [51], as shown in Fig. 1. The function $H(\boldsymbol{v})$ is the transmission function of a STDO and $\boldsymbol{v} = (x_v, y_v, \tau_v)^{\mathrm{T}}$ denotes an arbitrary spatiotemporal point at the plane of the object. Note that the transmission function of the STDO depends on both the spatial and temporal coordinates. For a spatiotemporal phenomenon, one can take either $m = 3$, which means that there are two transverse spatial dimensions and a temporal dimension, or $m = 2$, which means that there is only one transverse spatial dimension and a temporal dimension. If $m = 1$, it simply returns to the spatial ghost imaging [29] or interference [21], or temporal ghost imaging [43] or interference [41].

For simplicity, we assume that the STDO consists of very narrow slits (or apertures) controlled by shutters. At a certain time one shutter opens for one slit in a transverse position. When the shutter is open during a certain time, the light can pass through one slit (aperture) at a certain position, while when the shutter is closed, light is blocked. Therefore, the transmission function of the object is defined as

$$H(\boldsymbol{v}) = \begin{cases} 1, & \text{inside slit (or aperture) and shutter open,} \\ 0, & \text{outside slit (or aperture) or shutter closed.} \end{cases} \tag{8}$$

Specially, when the slit is extremely narrow, the object transmission function is further written as $H(\boldsymbol{v}) = \delta(\boldsymbol{v} - \boldsymbol{a}_1) + \delta(\boldsymbol{v} - \boldsymbol{a}_2)$, where δ denotes the Dirac delta function and $\boldsymbol{a}_i = (x_{ai}, y_{ai}, \tau_{ai})^{\mathrm{T}}$ is the spatiotemporal location of the slit. Here we consider only two slits at two different positions and times so one may refer this object as spatiotemporal dynamic double slits. In practical situations, a dynamic object may consist of a number of such slits (or apertures) with alternative open and close, and it can be seen as a "live" object in space and time. Such STDO is introduced here for spatiotemporal ghost imaging and interference technique, and this idea may open a door for the concept of "ghost video" by using the correlation information.

In order to analytically investigate the STGII, here the spatiotemporal light source is a kind of partially coherent Gaussian Schell-model pulsed beam, which can be written in the compact form of tensors as follows [49]:

$$\Gamma_0(\bar{\boldsymbol{r}}_0) = \exp\left[-\frac{ik}{2}\left(\bar{\boldsymbol{r}}_0^{\mathrm{T}}\overline{\boldsymbol{Q}}_{\mathrm{in}}^{-1}\bar{\boldsymbol{r}}_0\right)\right], \tag{9}$$

where $\bar{\boldsymbol{r}}_0 = \binom{\boldsymbol{r}_{10}}{\mathbf{r}_{20}}$ represents the two arbitrary spatiotemporal points at the source plane and $\overline{\boldsymbol{Q}}_{\mathrm{in}}^{-1} = \begin{pmatrix} \widetilde{\boldsymbol{\sigma}}_{1,} & \widetilde{\boldsymbol{\sigma}}_2 \\ \widetilde{\boldsymbol{\sigma}}_{2,} & \widetilde{\boldsymbol{\sigma}}_1 \end{pmatrix}$ is a $2m \times 2m$ matrix and the submatrices are $\widetilde{\boldsymbol{\sigma}}_1 = \begin{pmatrix} -\frac{i}{2k}\boldsymbol{\sigma}_{\mathrm{I}}^{-2} - \frac{i}{k}\boldsymbol{\sigma}_{\mathrm{cs}}^{-2}, & \mathbf{0}_2 \\ \mathbf{0}_{1,} & -\frac{i}{k}\sigma_\tau^{-2} - \frac{i}{k}\sigma_{\mathrm{ct}}^{-2} \end{pmatrix}$ and $\widetilde{\boldsymbol{\sigma}}_2 = \begin{pmatrix} \frac{i}{k}\boldsymbol{\sigma}_{\mathrm{cs}}^{-2}, & \mathbf{0}_2 \\ \mathbf{0}_{1,} & \frac{i}{k}\sigma_{\mathrm{ct}}^{-2} \end{pmatrix}$, which are $m \times m$ matrices. Here $\boldsymbol{\sigma}_s^{-2} = \begin{pmatrix} \sigma_s^{-2} & 0 \\ 0 & \sigma_s^{-2} \end{pmatrix}$ with the subscript $s = \mathrm{I}, \mathrm{cs}$ are the spatial properties of such pulsed beams, and $\mathbf{0}_2$ and $\mathbf{0}_1$ are $(m-1) \times 1$ and $1 \times (m-1)$ zero matrices, respectively. All notations σ_{I}, σ_{cs}, σ_τ, and σ_{ct} are positive constants, representing the spatial width, spatial coherence length, temporal width, and temporal coherence length of Gaussian Schell-model pulsed beams, respectively. By using the tensors method (see the Appendix for details), we can find the following analytical solution for ensemble averaged intensities at D1:

$$\langle I(\boldsymbol{\rho}_1)\rangle = \left|\left(\overline{\mathbf{A}}_1 + \overline{\mathbf{B}}_1\overline{\boldsymbol{Q}}_{\mathrm{in}}^{-1}\right)\right|^{-\frac{1}{2}} \times \exp\left\{-\frac{ik}{2}\left[-\bar{\boldsymbol{\rho}}_{11}^{\mathrm{T}}\overline{\mathbf{B}}_1^{-1}\left(\overline{\mathbf{A}}_1 + \overline{\mathbf{B}}_1\overline{\boldsymbol{Q}}_{\mathrm{in}}^{-1}\right)^{-1}\bar{\boldsymbol{\rho}}_{11}\right]\right\}, \tag{10}$$

and the intensity at D2

$$\langle I(\boldsymbol{\rho}_2 = 0)\rangle = \left(\frac{k}{2\pi}\right)^m\left[(-1)^m\left|\left(\overline{\mathbf{A}}_{21} + \overline{\mathbf{B}}_{21}\overline{\boldsymbol{Q}}_{\mathrm{in}}^{-1}\right)\overline{\mathbf{B}}_{22}\right|\right]^{-\frac{1}{2}} \times \sum_{p=1}^{2}\sum_{q=1}^{2}\exp\left[-\frac{ik}{2}\left(\bar{\boldsymbol{a}}_{pq}^{\mathrm{T}}\overline{\boldsymbol{Q}}_{\mathrm{out1}}\bar{\boldsymbol{a}}_{pq} + \bar{\boldsymbol{a}}_{pq}^{\mathrm{T}}\overline{\mathbf{B}}_{22}^{-1}\overline{\mathbf{A}}_{22}\bar{\boldsymbol{a}}_{pq}\right)\right], \tag{11}$$

where $\overline{\boldsymbol{Q}}_{\mathrm{out1}} = (\overline{\mathbf{C}}_{21} + \overline{\mathbf{D}}_{21}\overline{\mathbf{Q}}_{\mathrm{in}}^{-1})(\overline{\mathbf{A}}_{21} + \overline{\mathbf{B}}_{21}\overline{\boldsymbol{Q}}_{\mathrm{in}}^{-1})^{-1}$. Similarly, we can find the analytical solution for the first-order correlation function (see the Appendix for details). Consequently the generalized analytical solution for STGII of the STDO can be obtained as

$$|\Gamma(\boldsymbol{\rho}_1, \boldsymbol{\rho}_2 = 0)|^2 = \left(\frac{k}{2\pi}\right)^m\left[(-1)^m\left|\overline{\mathbf{A}} + \overline{\mathbf{B}}\overline{\boldsymbol{Q}}_{\mathrm{in}}^{-1}\right|\left|\widetilde{\mathbf{B}}_{22}\right|\right]^{-1} \times \left|\sum_{n=1}^{2}\exp\left[-\frac{ik}{2}\left(\overline{\boldsymbol{R}}_u^{\mathrm{T}}\overline{\boldsymbol{Q}}_{\mathrm{out2}}\overline{\boldsymbol{R}}_u - \boldsymbol{a}_u^{\mathrm{T}}\widetilde{\mathbf{B}}_{22}^{-1}\widetilde{\mathbf{A}}_{22}\boldsymbol{a}_u\right)\right]\right|^2. \tag{12}$$

Here $\overline{\boldsymbol{Q}}_{\mathrm{out2}} = (\overline{\mathbf{C}} + \overline{\mathbf{D}}\overline{\boldsymbol{Q}}_{\mathrm{in}}^{-1})(\overline{\mathbf{A}} + \overline{\mathbf{B}}\overline{\boldsymbol{Q}}_{\mathrm{in}}^{-1})^{-1}$; $\overline{\boldsymbol{R}}_u = \binom{\boldsymbol{\rho}_1}{\boldsymbol{a}_u}$ shows two arbitrary spatiotemporal points at the plane of detector D1 and at the object plane. $\overline{\mathbf{A}}$, $\overline{\mathbf{B}}$, $\overline{\mathbf{C}}$, and $\overline{\mathbf{D}}$ are $2m \times 2m$ spatiotemporal transmission matrices at both the path 1 and the path between source and object, defined as $\overline{\mathbf{A}} = \begin{pmatrix} \widetilde{\mathbf{A}}_1 & 0 \\ 0 & \widetilde{\mathbf{A}}_{21} \end{pmatrix}$, $\overline{\mathbf{B}} = \begin{pmatrix} \widetilde{\mathbf{B}}_1 & 0 \\ 0 & -\widetilde{\mathbf{B}}_{21} \end{pmatrix}$, $\overline{\mathbf{C}} = \begin{pmatrix} \widetilde{\mathbf{C}}_1 & 0 \\ 0 & -\widetilde{\mathbf{C}}_{21} \end{pmatrix}$, and $\overline{\mathbf{D}} = \begin{pmatrix} \widetilde{\mathbf{D}}_1 & 0 \\ 0 & \widetilde{\mathbf{D}}_{21} \end{pmatrix}$. Similarly, $\overline{\mathbf{A}}_j = \begin{pmatrix} \widetilde{\mathbf{A}}_j & 0 \\ 0 & \widetilde{\mathbf{A}}_j \end{pmatrix}$, $\overline{\mathbf{B}}_j = \begin{pmatrix} \widetilde{\mathbf{B}}_j & 0 \\ 0 & -\widetilde{\mathbf{B}}_j \end{pmatrix}$, $\overline{\mathbf{C}}_j = \begin{pmatrix} \widetilde{\mathbf{C}}_j & 0 \\ 0 & -\widetilde{\mathbf{C}}_j \end{pmatrix}$, and $\overline{\mathbf{D}}_j = \begin{pmatrix} \widetilde{\mathbf{D}}_j & 0 \\ 0 & \widetilde{\mathbf{D}}_j \end{pmatrix}$ are $2m \times 2m$ spatiotemporal transmission matrices of the relevant optical system as shown in Fig. 1. $\bar{\boldsymbol{\rho}}_{11} = \binom{\boldsymbol{\rho}_1}{\boldsymbol{\rho}_1}$ are the same spatiotemporal points at D1 and $\bar{\boldsymbol{a}}_{pq} = \binom{\boldsymbol{a}_p}{\boldsymbol{a}_q}$ are the spatiotemporal points at the object plane. When $p = q$, $\bar{\boldsymbol{a}}_{pq}$ represents the same spatiotemporal points; otherwise, it represents two different spatiotemporal points.

From the definition of visibility for ghost image introduced by Gatti *et al.* [23], we can write the expression of visibility for STGII as

$$V = \frac{|\Gamma(\boldsymbol{\rho}_1, \boldsymbol{\rho}_2 = 0)|^2_{\max}}{G^2(\boldsymbol{\rho}_1, \boldsymbol{\rho}_2 = 0)_{\max}}, \tag{13}$$

from which we can observe that the background terms have the main role in the visibility of ghost imaging and interference technique.

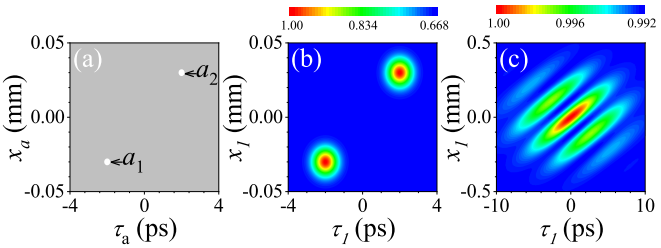

FIG. 2. (a) Spatiotemporal points of slits at the object plane. (b),(c) $G^{(2)}(\boldsymbol{\rho}_1, \boldsymbol{\rho}_2 = 0)/G^{(2)}(\boldsymbol{\rho}_1, \boldsymbol{\rho}_2 = 0)_{\max}$ as functions of spatial and temporal coordinates of D1, with spatiotemporal ghost image (b) and interference (c) at $z_1 = 30$ mm and 50 mm, respectively. Other parameters are $\sigma_I = 3$ mm, $\sigma_{cs} = 0.009$ mm, $\sigma_\tau = 35$ ps, $\sigma_{ct} = 0.6$ ps, $z_{21} = 30$ mm, $z_{22} = 20$ mm, $\omega = 2.691$ rad/fs, $n = 1.00027$, and $\beta_2 = 0.023835$ ps^{2}km^{-1}. For the object, the pointlike shutter opens at $(x_{a1}, \tau_{a1}) = (-0.03$ mm, -2 ps) and $(x_{a2}, \tau_{a2}) = (0.03$ mm, 2 ps).

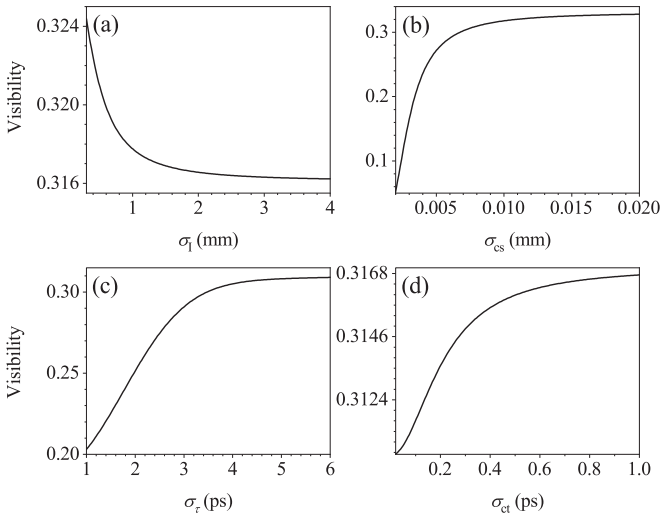

FIG. 3. Visibility of the spatiotemporal ghost image as functions of (a) σ_I, (b) σ_{cs}, (c) σ_τ, and (d) σ_{ct}. Other unmentioned parameters are the same as in Fig. 2.

The spatiotemporal transmission matrix for the homogeneous dispersive media can be given as [51]

$$\widetilde{\mathbf{A}} = \widetilde{\mathbf{D}} = E, \quad \widetilde{\mathbf{C}} = 0, \quad \widetilde{\mathbf{B}} = \begin{pmatrix} \frac{z}{n(\omega)} & 0 & 0 \\ 0 & \frac{z}{n(\omega)} & 0 \\ 0 & 0 & -4\pi^2\beta_2 c\omega z \end{pmatrix},$$

where E is the identity matrix, z is the thickness length, and β_2 is group-velocity dispersion of the medium.

III. RESULTS AND DISCUSSIONS

Now we are going to demonstrate the STGII of the lensless case with a numerical two-dimensional example, with the two dimensions being temporal coordinate and transversal spatial coordinate in x direction. The lensless ghost image and interference from generalized analytical results can be obtained by setting the relevant condition, i.e., $\widetilde{\mathbf{B}}_1 = \widetilde{\mathbf{B}}_{21}$ for ghost image [36,43] and $\widetilde{\mathbf{B}}_1 = \widetilde{\mathbf{B}}_{21} + \widetilde{\mathbf{B}}_{22}$ for ghost interference [21,41]. We assume that all optical paths are in the same dispersive medium, while air is chosen as a common example of the dispersive medium.

According to the abovementioned assumptions, two-dimensional spatiotemporal transfer matrices are $\widetilde{\mathbf{A}}_j = \begin{pmatrix} 1 & 0 \\ 0 & 1 \end{pmatrix}$, $\widetilde{\mathbf{B}}_j = \begin{pmatrix} z_j/n(\omega) & 0 \\ 0 & -4\pi^2\beta_2 c\omega z_j \end{pmatrix}$, $\widetilde{\mathbf{C}}_j = \begin{pmatrix} 0 & 0 \\ 0 & 0 \end{pmatrix}$, and $\widetilde{\mathbf{D}}_j = \begin{pmatrix} 1 & 0 \\ 0 & 1 \end{pmatrix}$, and z_1 and z_{21} are the distances from source plane to detector D1 and plane of object, respectively, and z_{22} is the distance from the object plane to detector D2.

Figure 2(a) shows the spatiotemporal dynamic double slits as a STDO. Two spatiotemporal slits appear on the shutter opening as shown by $\boldsymbol{a}_1$ and $\boldsymbol{a}_2$. Since all optical paths are considered in the same dispersive medium the abovementioned conditions for ghost imaging and interference can be written as (i) $z_1 = z_{21}$ and (ii) $z_1 = z_{21} + z_{22}$, respectively. Figure 2(b) illustrates the spatiotemporal ghost image of such a system in the form of spatiotemporal frames, which is the first key result of this work. If these frames appear on a screen one by one, according to the sequence of temporal coordinates, then this appearance is just like a video on the screen. The advantage of imaging STDOs will improve the applications of ghost imaging in biomedical optics and other fields. Beside, it will pave the path towards new research areas, e.g., "ghost video," spatiotemporal ghost imaging with entangled photons, hard x rays, and matter waves. On the other hand, spatiotemporal interference fringes are shown in Fig. 2(c), appearing as tilted peaks for such dynamic slits. The spatial and temporal fringes can be distinguished by observing the figure along the vertical and horizontal axis, respectively. Figure 2(c) is the second key result of this work, which is showing spatiotemporal ghost interference.

Properties of partially coherent Gaussian Schell-model pulsed beams, including σ_I, σ_{cs}, σ_τ, and σ_{ct}, reside in matrix $\overline{\boldsymbol{Q}}_{in}^{-1}$, which appears in background terms [Eqs. (10) and (11)] as well as in the first-order correlation [Eq. (12)] and ultimately participate in visibility [Eq. (13)]. Here the numerical results for the effect of source properties on the visibility of the ghost image are shown in Fig. 3. From Fig. 3(a), we can observe that, with increase in σ_I, the visibility of the spatiotemporal ghost image decreases. Figures 3(b)–3(d) show that the visibility increases with increase in σ_{cs}, σ_τ, and σ_{ct}. The highest value of visibility is well in agreement with the previous work for ghost imaging in the spatial domain with partially coherent light [29]. With adjusting the spatial parameters, the quality of the ghost image can be improved at the cost of visibility and vice versa, which satisfies the results mentioned in [29]. For temporal parameters the quality of the spatiotemporal image increases with increasing σ_τ and decreases with increasing σ_{ct}. As compared to ghost imaging in a spatial or temporal domain, the ghost imaging in the spatiotemporal domain with more choices of parameters will be helpful to improve the control on the visibility or quality of the spatiotemporal ghost image. To realize spatiotemporal ghost imaging experimentally, the choice of suitable parameters of the partially coherent pulsed beam is very important. Similar increasing and decreasing trends for the visibility of STGII can be found by using another definition of visibility introduced by Cao *et al.* [52].

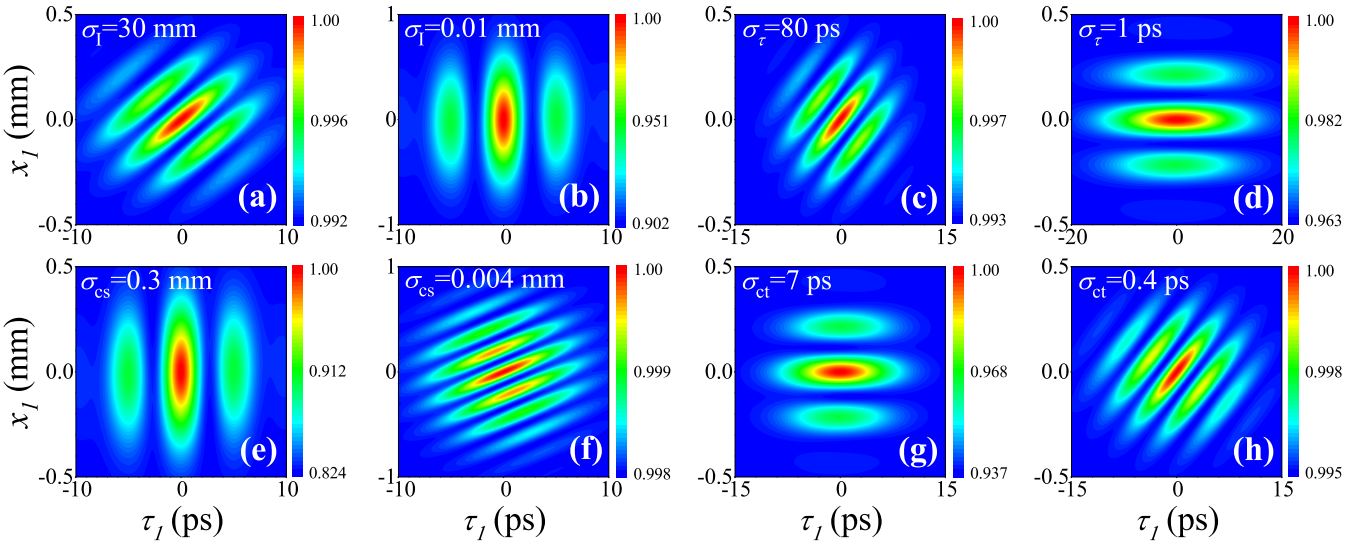

FIG. 4. Dependence of $G^{(2)}(\boldsymbol{\rho}_1, \boldsymbol{\rho}_2 = 0)/G^{(2)}(\boldsymbol{\rho}_1, \boldsymbol{\rho}_2 = 0)_{\max}$ on different values of (a),(b) σ_{I}, (c),(d) σ_τ, (e),(f) σ_{cs}, and (g),(h) σ_{ct} for spatiotemporal ghost interference. Other parameters are the same as in Fig. 2.

Cross terms in Eqs. (11) and (12) are mainly responsible for interference. Since matrix $\overline{\boldsymbol{Q}}_{\mathrm{in}}^{-1}$ appears in the cross terms, the source properties also participate in the number of fringes and in the background terms as shown in Fig. 4. In Figs. 4(a), 4(b) and 4(c), 4(d) by decreasing spatial and temporal width of the source, there is a decrease in the number of interference fringes in the spatial and temporal domain, respectively. Similarly, it is observed in Figs. 4(e), 4(f) and 4(g), 4(h) that, by decreasing the spatial and temporal coherence length of the source, an increase occurs in the number of interference fringes in the spatial and temporal domain, respectively. There are similar effects of a decrease or an increase in the background terms [see the color bars of Figs. 4(a), 4(b), 4(c), 4(d), and Figs. 4(e), 4(f), 4(g), 4(h), respectively]. The decrease in the background terms will increase the visibility and vice versa. Thus it concludes that by decreasing spatial or temporal width or by increasing spatial or temporal coherence length of the source, the visibility of spatiotemporal ghost interference can increase up to a certain value.

For realizing STGII experimentally one can follow the scheme as shown in Fig. 1. Since spatiotemporal Bessel pulsed beams have been realized experimentally [53], one may follow a similar experimental scheme for producing spatiotemporal Gaussian Shell-model pulsed beams. The spatiotemporal dynamic double slits may be produced by using double slits covered by a pair of automechanical shutters. Both the shutters should have the ability to open and close with predefined time. The spatiotemporal dynamic object may also be realized by using an ultrafast electro-optic modulator driven by a spatial-dependent electrode. Here we suggest that the detector D1 may consist of an array of fast-response photodiodes with high-time resolution compared with the source duration and it also provides the spatial information from each individual photodiode, and the detector D2 is a slow-response photodiode and does not need to provide the spatial information. It has been pointed out that the effective fluctuation time of the source should be equal to half of the fastest time variation that one wants to resolve in the object [44].

IV. CONCLUSION

In conclusion, we have introduced the STGII technique as an advancement in the conventional ghost imaging, for imaging the STDOs. Spatiotemporal dynamic double slits are introduced to mimic live objects. By using a partially coherent Gaussian Schell-model pulsed beam as a source field we find the generalized analytical expressions for STGII for spatiotemporal dynamic double slits. Furthermore, with this advancement we show numerically the spatiotemporal ghost images and interference patterns for the lensless case, from which we discuss the influence of source pulsed beam properties in the number of interference fringes, background terms, and in the visibility of the spatiotemporal ghost image and interference. We also observe that, by using spatiotemporal partially coherent sources, the selection of suitable beam parameters is important for controlling the visibility of spatiotemporal ghost image and interference patterns. The advantage of imaging STDOs will improve the applications of ghost imaging in biomedical optics and other fields, which will increase the general interest of ghost imaging and pave the path towards new areas of research, e.g., "ghost video," spatiotemporal ghost imaging with entangled photons, hard x rays, and matter waves.

ACKNOWLEDGMENTS

This research is supported by the National Natural Science Foundation of China (Grants No. 11674284 and No. 11974309), Zhejiang Provincial Natural Science Foundation of China under Grant No. LD18A040001, National Key Research and Development Program of China (Grant No. 2017YFA0304202), and the Fundamental Research Funds for the Center Universities (Grant No. 2019FZA3005).

APPENDIX: DERIVATION OF EQS. (10)–(12)

Here we will explain how to find the ensemble averaged intensities at detectors D1 and D2, and the first-order correlation between both detectors. By using the definition of spatiotemporal dynamic double slits one can get the analytical solutions as explained below.

1. Propagation equation for intensity at detector D1

By using Eq. (2) and Eq. (4) we can find the intensity at D1 as

$$\langle I(\boldsymbol{\rho}_1)\rangle = \left(\frac{k}{2\pi}\right)^m [\det(\widetilde{\mathbf{B}}_1)\det(\widetilde{\mathbf{B}}_1)]^{-\frac{1}{2}} \iiint\iiint d^3r_{10}d^3r_{20}\Gamma_0(\boldsymbol{r}_{10},\boldsymbol{r}_{20}) \times \exp\left\{-\frac{ik}{2}\left[\left(\boldsymbol{r}_{10}^{\mathrm{T}}\widetilde{\mathbf{B}}_1^{-1}\widetilde{\mathbf{A}}_1\boldsymbol{r}_{10} - 2\boldsymbol{r}_{10}^{\mathrm{T}}\widetilde{\mathbf{B}}_1^{-1}\boldsymbol{\rho}_1 + \boldsymbol{\rho}_1^{\mathrm{T}}\widetilde{\mathbf{D}}_1\widetilde{\mathbf{B}}_1^{-1}\boldsymbol{\rho}_1\right) - \left(\boldsymbol{r}_{20}^{\mathrm{T}}\widetilde{\mathbf{B}}_1^{-1}\widetilde{\mathbf{A}}_1\boldsymbol{r}_{20} - 2\boldsymbol{r}_{20}^{\mathrm{T}}\widetilde{\mathbf{B}}_1^{-1}\boldsymbol{\rho}_1 + \boldsymbol{\rho}_1^{\mathrm{T}}\widetilde{\mathbf{D}}_1\widetilde{\mathbf{B}}_1^{-1}\boldsymbol{\rho}_1\right)\right]\right\}. \tag{A1}$$

We can write Eq. (A1) in the most compact form of tensors as follows:

$$\langle I(\boldsymbol{\rho}_1)\rangle = \left(\frac{k}{2\pi}\right)^m [(-1)^m\det(\overline{\mathbf{B}}_1)]^{-\frac{1}{2}} \iiint\iiint d^3r_{10}d^3r_{20}\Gamma_0(\bar{\boldsymbol{r}}_0)\exp\left[-i\frac{k}{2}\begin{pmatrix}\bar{\boldsymbol{r}}_0\\ \bar{\boldsymbol{\rho}}_{11}\end{pmatrix}^{\mathrm{T}}\begin{pmatrix}\overline{\mathbf{B}}_1^{-1}\overline{\mathbf{A}}_1 & -\overline{\mathbf{B}}_1^{-1}\\ \overline{\mathbf{C}}_1 - \overline{\mathbf{D}}_1\overline{\mathbf{B}}_1^{-1}\overline{\mathbf{A}}_1 & \overline{\mathbf{D}}_1\overline{\mathbf{B}}_1^{-1}\end{pmatrix}\begin{pmatrix}\bar{\boldsymbol{r}}_0\\ \bar{\boldsymbol{\rho}}_{11}\end{pmatrix}\right]. \tag{A2}$$

By putting Eq. (9) in Eq. (A2), after solving the integral one can get Eq. (10).

2. Propagation equation for intensity at detector D2

By using Eq. (2) and Eq. (5) we can find the intensity at D2 as

$$\langle I(\boldsymbol{\rho}_2)\rangle = \left(\frac{k}{2\pi}\right)^{2m} [\det(\widetilde{\mathbf{B}}_2)\det(\widetilde{\mathbf{B}}_3)\det(\widetilde{\mathbf{B}}_2)\det(\widetilde{\mathbf{B}}_3)]^{-\frac{1}{2}} \iiiint\iiiint\iiiint d^3r_{10}d^3r_{20}d^3v_1d^3v_2\Gamma_0(\boldsymbol{r}_{10},\boldsymbol{r}_{20})H(\boldsymbol{v}_1)H^*(\boldsymbol{v}_2)$$
$$\times \exp\left\{-\frac{ik}{2}\left[\left(\boldsymbol{r}_{10}^{\mathrm{T}}\widetilde{\mathbf{B}}_2^{-1}\widetilde{\mathbf{A}}_2\boldsymbol{r}_{10} - 2\boldsymbol{r}_{10}^{\mathrm{T}}\widetilde{\mathbf{B}}_2^{-1}\boldsymbol{v}_1 + \boldsymbol{v}_1^{\mathrm{T}}\widetilde{\mathbf{D}}_2\widetilde{\mathbf{B}}_2^{-1}\boldsymbol{v}_1\right) + \left(\boldsymbol{v}_1^{\mathrm{T}}\widetilde{\mathbf{B}}_3^{-1}\widetilde{\mathbf{A}}_3\boldsymbol{v}_1 - 2\boldsymbol{v}_1^{\mathrm{T}}\widetilde{\mathbf{B}}_3^{-1}\boldsymbol{\rho}_2 + \boldsymbol{\rho}_2^{\mathrm{T}}\widetilde{\mathbf{D}}_3\widetilde{\mathbf{B}}_3^{-1}\boldsymbol{\rho}_2\right)\right]\right\}$$
$$\times \exp\left\{\frac{ik}{2}\left[\left(\boldsymbol{r}_{20}^{\mathrm{T}}\widetilde{\mathbf{B}}_2^{-1}\widetilde{\mathbf{A}}_2\boldsymbol{r}_{20} - 2\boldsymbol{r}_{20}^{\mathrm{T}}\widetilde{\mathbf{B}}_2^{-1}\boldsymbol{v}_2 + \boldsymbol{v}_2^{\mathrm{T}}\widetilde{\mathbf{D}}_2\widetilde{\mathbf{B}}_2^{-1}\boldsymbol{v}_2\right) + \left(\boldsymbol{v}_2^{\mathrm{T}}\widetilde{\mathbf{B}}_3^{-1}\widetilde{\mathbf{A}}_3\boldsymbol{v}_2 - 2\boldsymbol{v}_2^{\mathrm{T}}\widetilde{\mathbf{B}}_3^{-1}\boldsymbol{\rho}_2 + \boldsymbol{\rho}_2^{\mathrm{T}}\widetilde{\mathbf{D}}_3\widetilde{\mathbf{B}}_3^{-1}\boldsymbol{\rho}_2\right)\right]\right\}. \tag{A3}$$

We can write Eq. (A3) in the most compact form of tensors as follows:

$$\langle I(\boldsymbol{\rho}_2)\rangle = \left(\frac{k}{2\pi}\right)^{2m} [(-1)^{2m}\det(\overline{\mathbf{B}}_2\overline{\mathbf{B}}_3)]^{-\frac{1}{2}} \iiiint\iiiint\iiiint d^3r_{10}d^3r_{20}d^3v_1d^3v_2\Gamma_0(\bar{\boldsymbol{r}}_0)H(\boldsymbol{v}_1)H^*(\boldsymbol{v}_2)$$
$$\times \exp\left\{-i\frac{k}{2}\left[\begin{pmatrix}\bar{\boldsymbol{r}}_0\\ \bar{\boldsymbol{v}}\end{pmatrix}^{\mathrm{T}}\begin{pmatrix}\overline{\mathbf{B}}_2^{-1}\overline{\mathbf{A}}_2 & -\overline{\mathbf{B}}_2^{-1}\\ \overline{\mathbf{C}}_2 - \overline{\mathbf{D}}_2\overline{\mathbf{B}}_2^{-1}\overline{\mathbf{A}}_2 & \overline{\mathbf{D}}_2\overline{\mathbf{B}}_2^{-1}\end{pmatrix}\begin{pmatrix}\bar{\boldsymbol{r}}_0\\ \bar{\boldsymbol{v}}\end{pmatrix} + \begin{pmatrix}\bar{\boldsymbol{v}}\\ \bar{\boldsymbol{\rho}}_{22}\end{pmatrix}^{\mathrm{T}}\begin{pmatrix}\overline{\mathbf{B}}_3^{-1}\overline{\mathbf{A}}_3 & -\overline{\mathbf{B}}_3^{-1}\\ \overline{\mathbf{C}}_3 - \overline{\mathbf{D}}_3\overline{\mathbf{B}}_3^{-1}\overline{\mathbf{A}}_3 & \overline{\mathbf{D}}_3\overline{\mathbf{B}}_3^{-1}\end{pmatrix}\begin{pmatrix}\bar{\boldsymbol{v}}\\ \bar{\boldsymbol{\rho}}_{22}\end{pmatrix}\right]\right\}. \tag{A4}$$

By putting Eq. (9) in Eq. (A4), after solving the integral one can get Eq. (11).

3. Propagation equation for the first-order correlation function

By using Eqs. (3)–(7) we can find the first-order correlation function at two different spatiotemporal points as

$$\Gamma(\boldsymbol{\rho}_1,\boldsymbol{\rho}_2) = \left(\frac{ik}{2\pi}\right)^{\frac{3m}{2}} [\det(\widetilde{\mathbf{B}}_1)\det(\widetilde{\mathbf{B}}_2)\det(\widetilde{\mathbf{B}}_3)]^{-\frac{1}{2}} \iiint\iiint\iiint d^3r_{10}d^3r_{20}d^3v_2\Gamma_0(\boldsymbol{r}_{10},\boldsymbol{r}_{20})H^*(\boldsymbol{v}_2)$$
$$\times \exp\left\{-\frac{ik}{2}\left[\left(\boldsymbol{r}_{10}^{\mathrm{T}}\widetilde{\mathbf{B}}_1^{-1}\widetilde{\mathbf{A}}_1\boldsymbol{r}_{10} - 2\boldsymbol{r}_{10}^{\mathrm{T}}\widetilde{\mathbf{B}}_1^{-1}\boldsymbol{\rho}_1 + \boldsymbol{\rho}_1^{\mathrm{T}}\widetilde{\mathbf{D}}_1\widetilde{\mathbf{B}}_1^{-1}\boldsymbol{\rho}_1\right) - \left(\boldsymbol{r}_{20}^{\mathrm{T}}\widetilde{\mathbf{B}}_2^{-1}\widetilde{\mathbf{A}}_2\boldsymbol{r}_{20} - 2\boldsymbol{r}_{20}^{\mathrm{T}}\widetilde{\mathbf{B}}_2^{-1}\boldsymbol{v}_2 + \boldsymbol{v}_2^{\mathrm{T}}\widetilde{\mathbf{D}}_2\widetilde{\mathbf{B}}_2^{-1}\boldsymbol{v}_2\right)\right]\right\}$$
$$\times \exp\left[\frac{ik}{2}\left(\boldsymbol{v}_2^{\mathrm{T}}\widetilde{\mathbf{B}}_3^{-1}\widetilde{\mathbf{A}}_3\boldsymbol{v}_2 - 2\boldsymbol{v}_2^{\mathrm{T}}\widetilde{\mathbf{B}}_3^{-1}\boldsymbol{\rho}_2 + \boldsymbol{\rho}_2^{\mathrm{T}}\widetilde{\mathbf{D}}_3\widetilde{\mathbf{B}}_3^{-1}\boldsymbol{\rho}_2\right)\right]. \tag{A5}$$

We can write Eq. (A5) in the most compact form of tensors as follows:

$$\Gamma(\boldsymbol{\rho}_1,\boldsymbol{\rho}_2)=\left(\frac{ik}{2\pi}\right)^{\frac{3m}{2}}[(-1)^m\det(\overline{\mathbf{B}})\det(\widetilde{\mathbf{B}}_3)]^{-\frac{1}{2}}\iiint\iiint\iiint d^3r_{10}d^3r_{20}d^3v_2\Gamma_0(\bar{\boldsymbol{r}}_0)H^*(\boldsymbol{v}_2)$$
$$\times\exp\left[-i\frac{k}{2}\begin{pmatrix}\bar{\boldsymbol{r}}_0\\ \bar{\boldsymbol{\delta}}_{12}\end{pmatrix}^{\mathrm{T}}\begin{pmatrix}\overline{\mathbf{B}}^{-1}\overline{\mathbf{A}} & -\overline{\mathbf{B}}^{-1}\\ \overline{\mathbf{C}}-\overline{\mathbf{D}}\overline{\mathbf{B}}^{-1}\overline{\mathbf{A}} & \overline{\mathbf{D}}\overline{\mathbf{B}}^{-1}\end{pmatrix}\begin{pmatrix}\bar{\boldsymbol{r}}_0\\ \bar{\boldsymbol{\delta}}_{12}\end{pmatrix}\right]\exp\left[\frac{ik}{2}\left(\boldsymbol{v}_2^{\mathrm{T}}\widetilde{\mathbf{B}}_3^{-1}\widetilde{\mathbf{A}}_3\boldsymbol{v}_2-2\boldsymbol{v}_2^{\mathrm{T}}\widetilde{\mathbf{B}}_3^{-1}\boldsymbol{\rho}_2+\boldsymbol{\rho}_2^{\mathrm{T}}\widetilde{\mathbf{D}}_3\widetilde{\mathbf{B}}_3^{-1}\boldsymbol{\rho}_2\right)\right]. \tag{A6}$$

By putting Eq. (9) in Eq. (A6), after solving the integral one can get Eq. (12).

[1] T. B. Pittman, Y. H. Shih, D. V. Strekalov, and A. V. Sergienko, Phys. Rev. A **52**, R3429(R) (1995).
[2] D. V. Strekalov, A. V. Sergienko, D. N. Klyshko, and Y. H. Shih, Phys. Rev. Lett. **74**, 3600 (1995).
[3] B. I. Erkmen and J. H. Shapiro, Adv. Opt. Photon. **2**, 405 (2010).
[4] G. A. Barbosa, Phys. Rev. A **54**, 4473 (1996).
[5] A. Gatti, E. Brambilla, L. A. Lugiato, and M. I. Kolobov, Phys. Rev. Lett. **83**, 1763 (1999).
[6] B. E. A. Saleh, A. F. Abouraddy, A. V. Sergienko, and M. C. Teich, Phys. Rev. A **62**, 043816 (2000).
[7] A. Gatti, E. Brambilla, and L. A. Lugiato, Phys. Rev. Lett. **90**, 133603 (2003).
[8] A. F. Abouraddy, B. E. A. Saleh, A. V. Sergienko, and M. C. Teich, Opt. Express **9**, 498 (2001).
[9] A. F. Abouraddy, B. E. A. Saleh, A. V. Sergienko, and M. C. Teich, Phys. Rev. Lett. **87**, 123602 (2001).
[10] D. Pelliccia, A. Rack, M. Scheel, V. Cantelli, and D. M. Paganin, Phys. Rev. Lett. **117**, 113902 (2016).
[11] H. Yu, R. Lu, S. Han, H. Xie, G. Du, T. Xiao, and D. Zhu, Phys. Rev. Lett. **117**, 113901 (2016).
[12] R. I. Khakimov, B. M. Henson, D. K. Shin, S. S. Hodgman, R. G. Dall, K. G. H. Baldwin, and A. G. Truscott, Nature (London) **540**, 100 (2016).
[13] S. S. Hodgman, W. Bu, S. B. Mann, R. I. Khakimov, and A. G. Truscott, Phys. Rev. Lett. **122**, 233601 (2019).
[14] S. Li, F. Cropp, K. Kabra, T. J. Lane, G. Wetzstein, P. Musumeci, and D. Ratner, Phys. Rev. Lett. **121**, 114801 (2018).
[15] K. Chen and S. Han, arXiv:1801.10046.
[16] A. F. Abouraddy, B. E. A. Saleh, A. V. Sergienko, and M. C. Teich, J. Opt. Soc. Am. B **19**, 1174 (2002).
[17] R. S. Bennink, S. J. Bentley, and R. W. Boyd, Phys. Rev. Lett. **89**, 113601 (2002).
[18] R. S. Bennink, S. J. Bentley, R. W. Boyd, and J. C. Howell, Phys. Rev. Lett. **92**, 033601 (2004).
[19] A. Gatti, E. Brambilla, M. Bache, and L. A. Lugiato, Phys. Rev. Lett. **93**, 093602 (2004).
[20] A. Gatti, E. Brambilla, M. Bache, and L. A. Lugiato, Phys. Rev. A **70**, 013802 (2004).
[21] Y. Cai and S. Y. Zhu, Opt. Lett. **29**, 2716 (2004).
[22] F. Ferri, D. Magatti, A. Gatti, M. Bache, E. Brambilla, and L. A. Lugiato, Phys. Rev. Lett. **94**, 183602 (2005).
[23] A. Gatti, M. Bache, D. Magatti, E. Brambilla, F. Ferri, and L. A. Lugiato, J. Mod. Opt. **53**, 739 (2006).
[24] B. I. Erkmen and J. H. Shapiro, Phys. Rev. A **77**, 043809 (2008).
[25] A. Valencia, G. Scarcelli, M. DAngelo, and Y. Shih, Phys. Rev. Lett. **94**, 063601 (2005).
[26] D. Zhang, Y. Zhai, L. Wu, and X. Chen, Opt. Lett. **30**, 2354 (2005).
[27] G. Scarcelli, V. Berardi, and Y. Shih, Appl. Phys. Lett. **88**, 061106 (2006).
[28] M. Bache, D. Magatti, F. Ferri, A. Gatti, E. Brambilla, and L. A. Lugiato, Phys. Rev. A **73**, 053802 (2006).
[29] Y. Cai and S. Y. Zhu, Phys. Rev. E **71**, 056607 (2005).
[30] L. Basano and P. Ottonello, Appl. Phys. Lett. **89**, 091109 (2006).
[31] M. Zhang, Q. Wei, X. Shen, Y. Liu, H. Liu, J. Cheng, and S. Han, Phys. Rev. A **75**, 021803(R) (2007).
[32] S. Crosby, S. Castelletto, C. Aruldoss, R. E. Scholten, and A. Roberts, New J. Phys. **9**, 285 (2007).
[33] H. Liu and S. Han, Opt. Lett. **33**, 824 (2008).
[34] F. Ferri, D. Magatti, V. G. Sala, and A. Gatti, Appl. Phys. Lett. **92**, 261109 (2008).
[35] Y. Cai, Q. Lin, and O. Korotkova, Opt. Express **17**, 2453 (2009).
[36] L. G. Wang, S. Qamar, S. Y. Zhu, and M. S. Zubairy, Phys. Rev. A **79**, 033835 (2009).
[37] M. Luo, W. Zhu, and D. Zhao, Phys. Lett. A **379**, 2789 (2015).
[38] Y. Si, L. J. Kong, Y. N. Li, C. H. Tu, and H. T. Wang, Chin. Phys. Lett. **33**, 034203 (2016).
[39] M. Bellini, F. Marin, S. Viciani, A. Zavatta, and F. T. Arecchi, Phys. Rev. Lett. **90**, 043602 (2003).
[40] S. Viciani, A. Zavatta, and M. Bellini, Phys. Rev. A **69**, 053801 (2004).
[41] V. Torres-Company, H. Lajunen, J. Lancis, and A. T. Friberg, Phys. Rev. A **77**, 043811 (2008).
[42] T. Setälä, T. Shirai, and A. T. Friberg, Phys. Rev. A **82**, 043813 (2010).
[43] T. Shirai, T. Setälä, and A. T. Friberg, J. Opt. Soc. Am. B **27**, 2549 (2010).
[44] P. Ryczkowski, M. Barbier, A. T. Friberg, J. M. Dudley, and G. Genty, Nat. Photon. **10**, 167 (2016).
[45] P. Ryczkowski, M. Barbier, A. T. Friberg, J. M. Dudley, and G. Genty, APL Photon. **2**, 046102 (2017).
[46] J. Liu, J. Wang, H. Chen, H. Zheng, Y. Liu, Y. Zhou, F. L. Li, and Z. Xu, Opt. Commun. **410**, 824 (2018).
[47] L. Qu, Y. Bai, S. Nan, Q. Shen, H. Li, and X. Fu, Opt. Laser Technol. **104**, 197 (2018).
[48] W. Zhang, D. Zhang, X. Qiu, and L. Chen, Phys. Rev. A **100**, 043832 (2019).
[49] L. Mandel and E. Wolf, *Optical Coherence and Quantum Optics* (Cambridge University Press, New York, 1995).
[50] L. G. Wang, Q. Lin, H. Chen, and S. Y. Zhu, Phys. Rev. E **67**, 056613 (2003).
[51] S. Wang and D. Zhao, *Matrix Optics* (Springer, Berlin, 2000).
[52] D. Z. Cao, J. Xiong, S. H. Zhang, L. F. Lin, L. Gao, and K. Wang, Appl. Phys. Lett. **92**, 201102 (2008).
[53] M. Dallaire, N. McCarthy, and M. Piche, Opt. Express **17**, 18148 (2009).